High order harmonic balance formulation of free and encapsulated microbubbles

Marie-Christine Pauzin, Serge Mensah *, Bruno Cochelin, Jean-Pierre Lefebvre

CNRS - Laboratoire de Mécanique et d'Acoustique, 31 chemin Joseph Aiguier, 13402 Marseille, Cedex 20, France

ARTICLE INFO

ABSTRACT

The radial responses of free and encapsulated microbubbles excited by an ultrasonic plane wave with a large wavelength in comparison with the bubble size are governed by NonLinear Ordinary Differential Equations (NL-ODEs). The nonlinear frequency response gives the harmonic content of the time response and constitutes the expected outcome of a high order harmonic analysis. In this paper, high order harmonic balance analysis of modified "RPNNP" (bubble), Hoff and Marmottant (contrast agents) models is performed with an open-source software program. For this purpose, the original NL-ODEs are recast into nonlinear systems in which the nonlinearities are at most quadratic. In the spectral domain, this recast provides close form and aliasing-free solutions of arbitrarily large numbers of harmonics. Relevant quantities such as primary and secondary resonances and the nonlinear amplitude threshold of the excitation wave are evaluated. The frequency curves drawn up characterize the bending and quantify the jump frequencies and amplitudes of each harmonic component. The results obtained with this predictive method confirm that it should provide a useful tool for nonlinear bubble detection and sizing and for contrast agent designing.

© 2010 Elsevier Ltd. All rights reserved.

1. Introduction

Studies on the nonlinear responses of microbubbles to ultrasound excitations have many applications, including the detection and sizing of bubbles [1–6] in environmental (ocean) contexts [7,8], and in the field of engineering [9,10], they range from the propeller damage induced by cavitation to drag reduction by supercavitation [11,12], valve leakage, chemical process control [13], and the monitoring of liquid sodium coolant for nuclear reactors [14,15]. In the biomedical field, they include the prevention of decompression sickness (in extravehicular diving and space activities [16]) and medical imaging with contrast agents (i.e. encapsulated microbubbles) [17–19,21–26]. In the latter field, it has been established that under specific conditions, the sole second harmonic signal generated by bubbles and Ultrasonic Contrast Agents (UCAs) can yield enhanced contrast information (for bubble/tissue discrimination purposes) in comparison with the global signal containing the fundamental component. This application to bubble/tissue discrimination using the second harmonic is based on the fact that the nonlinear responses of tissues are much weaker than those of bubbles and contrast agents. The second harmonic imaging potential of UCAs has been thoroughly investigated by a number of research institutions and private companies in order to determine relevant physical parameters for improving the second harmonic backscattering cross section. However, in practice, second harmonic imaging methods have several drawbacks: first, the data/images are altered by an attenuation of the second harmonic components greater than that undergone by the

---

* Corresponding author. Tel.: +33 4 911 641 98; fax: +33 4 911 642 70.
  E-mail address: mensah@lma.cnrs-mrs.fr (S. Mensah).

fundamental one, which reduces the range (the depth of penetration) of the second harmonic imaging. Second, since commercial ultrasound scanners use relatively large output power (Mechanical Index, MI > 0.3), the significant second harmonic signal produced by the tissue itself impinges on the contrast of the bubbles or agents [27–30]. It has been established in particular [31] that the level of tissue harmonics due to nonlinear propagation depends mainly on the peak pressure but not on the pulse energy. In tissues, for example, chirp excitation produces significantly fewer harmonics than equal energy pulses: in the case of the second harmonic, the difference can be greater than 10 dB [32]. However, due to the "damped behavior" (hysteresis) of bubbles, their responses depend on both the peak amplitude and the pulse length, and chirp excitation causes larger bubble wall excursions than equal amplitude pulses. Therefore, in the B-mode image, a 10-dB improvement in the signal to noise ratio (SNR) is obtained [32]. Nonetheless, the challenge in ultrasound contrast imaging is how to discriminate more clearly between the perfused tissue and the contrast bubbles: this possibility is usually expressed by the Contrast to Tissue Ratio (CTR). It has been reported that bubbles generate more energy at sub/higher harmonics than tissues, especially in low frequency transmissions [33]. The CTRs obtained with a dual frequency probe (0.9, 2.96 MHz) reached high levels at the super harmonic frequencies (third–fourth–fifth) up to 50 dB, whereas the CTRs obtained with a normal probe operating in the second harmonic mode gave values at least 30 dB lower [34]. However, the main drawbacks with super harmonic imaging are the poor sensitivity and the SNR: since super harmonics involve less energy than that occurring at second harmonic level, the detection of bubbles is more susceptible to background noise. Subharmonic signals have a higher signal to background noise ratio than the second harmonics [35,36]. In addition, in order to prevent tissues from being damaged by cavitation, the use of non-destructive contrast agent imaging is currently being envisaged for blood flow assessment purposes. In this context, low Mechanical Index (MI < 0.1) approaches are required which minimize not only the image artifacts due to NL propagation but also the NL bubble echoes, which degrade both the SNR and CTR. This issue could be partly solved if it was possible to use most of the major harmonics, ultraharmonics and subharmonics generated by the pulsating bubbles. The detection capacity, the range and the resolution of these methods might be improved by using specific coded sequences (pulse compression techniques). Also, the bubble (and contrast agent) signature characterization might be enhanced by using a time–frequency representation of the global response (including the fundamental). A technique based on Golay phase encoding, Pulse Inversion, and Amplitude Modulation (GPIAM) was recently developed for performing contrast imaging with ultrasounds. A 12-dB improvement in the CTR was obtained using an 8-chip GPIAM sequence in comparison with a conventional Pulse Inversion (PI) method, and a 6.5-dB increase in the CTR was observed in comparison with a Pulse Inversion Amplitude Modulation (PIAM) sequence [37].

Given the importance of large bubble oscillations at resonance frequencies, it was therefore proposed to characterize the nonlinear acoustical responses of bubbles depending on the local context. This should pave the way to designing fairly accurate inversion procedures yielding information about the bubble size, the possible attachment of the contrast agent targeting neighboring tissues and the mechanical behavior of these neighboring tissues, for instance. In order to distinguish more clearly between the bubbles/tissues and improve their detection and characterization, nonlinear frequency responses of bubbles and contrast agents were obtained using various models and a high order Harmonic Balance Method (HBM) combined with a Continuation Method. This method, which was implemented in a software suite [38], has been described in detail in a previous paper [39]. It gives highly accurate approximations of the full responses, including stable and unstable solutions, the accuracy of which depends on the number (which can be large) of harmonic terms in the driving source involved. From the practical point of view, only a little experience in the field of bubble dynamics is required to be able to define the stable branches.

Since the main features of nonlinear as well as those of linear acoustic responses of microbubbles to ultrasound lie in their radial oscillations, this paper, like most of the literature on the subject, focuses on the radial oscillations of bare and coated spherical microbubbles. At least as far as stable oscillations are concerned, the main difference between models is the type of damping (thermal loss, radiation damping, fluid viscosity, shell buckling, etc.) involved. In the case of bare bubbles, modeling the problem leads to the so-called Rayleigh–Plesset equation and its generalization, the RPNNP model (referring to Rayleigh, Plesset, Nolting, Neppiras and Poritsky: the term was suggested by Lauterborn) [40] and its corrected form (including sound radiation) [41] or its alternative in terms of the Keller–Miksis model [42]. In the case of coated bubbles, modeling leads to equivalent equations that differ in terms of the shell behavior (the viscosity, hyperelasticity, etc.). Among the various models for the agents, one might quote those developed by Church [19], Hoff et al. [21] and Marmottant et al. [23]. In the corresponding NonLinear Ordinary Differential Equations (NL-ODEs) thus obtained, the time evolution of the radius of the bubble depends on the ultrasonic load. In most cases, the harmonic activation produced by an incident harmonic ultrasonic plane wave has been studied. When the amplitudes of the oscillations are not too large, classical perturbation methods [43,44] can be used, and these have been applied to solve these NL-ODEs, resulting in a small parameter dependency and control. This category of studies includes many analytical methods based on low order (second or third) approximations, such as those presented in the pioneering (and surprisingly rarely cited) paper by Nayfeh and Saric [45], who used a multiple scale method to obtain frequency responses showing the same "softening" behavior as bubbles. The simplicity of the parametrization procedure has given rise to great interest in this method, which was used by several authors [46,47], whereas Prosperetti [48] used another classical perturbation method, the Averaging Method. Again with a view to simulating the frequency responses, second-order small parameter combined with second-order harmonic balance developments was used by many authors such as Church [19] and Khismatullin and Nadim [49] in order to find explicit expressions. In line with Lauterborn [40], other authors chose the opposite approach

consisting of the full numerical resolution in the time-domain, followed by a Fourier analysis in order to extract the transfer function: [42,50] and more recently [22,24–26,51]. The method based on the purely numerical resolution of the time-domain ODE is currently the only method giving a highly accurate approximation of the solution. However, this approach yields only the stable solutions of the equations, and looking for hysteretic solutions and for each harmonic and sub-harmonic component of the response is not an easy task. A Harmonic Balance Method without any small-parameter developments is a more suitable means of high accuracy frequency response assessment. However, when the oscillations are large, i.e., when there are resonances, a development with a high number of harmonics is required to obtain a sufficiently high level of accuracy. Since the explicit balancing of a large number (a number greater than or equal to two) of harmonics is rather cumbersome, an automated balancing technique was employed here. This approach, in which a Harmonic Balance Method (HBM) was combined with a Continuation Method in the framework of Asymptotic Numerical Methods (ANMs) [52], was described in detail in a previous paper [39]. It resulted in an interactive, free, open access software program written for the Matlab® environment, named Manlab® [38]. This software program was consistently used in the present study to model three kinds of microbubbles: the RPNNP model [40] and a modified version of this model (taking radiation losses into account) [41,53] focusing on the free microbubble responses and two other models describing thinly encapsulated microbubbles. The first model of the latter kind, which was developed by Hoff et al. [21], was a thin-shell version of the Church model [19], and the second one, which was developed by Marmottant et al. [23], accounts for buckling and rupture. The latter model is restricted here, however, to the elastic behavior of the shell. These two models are known to be appropriate for simulating the latest generation of UCAs, polymer-shelled contrast agents and lipid-shelled contrast agents, respectively.

In the present numerical experiments, it is assumed that the radial nonlinear behavior of the microbubble or the contrast agent is sufficiently well characterized by its first three components (the fundamental plus two harmonics). The expansion of the solutions is in fact performed on the first four harmonics, to which we add the null frequency component. In practice, this should suffice when the attenuation coefficient of the host medium is linearly dependent on the depth at which the bubble is located and on the frequency, as in the case of "soft" tissues in biomedical engineering. Free bubbles in water may require performing a higher Fourier decomposition to be modeled with reasonably good accuracy because of the low viscosity of water, which reduces the absorption process. The dedicated software used here was based on a simple quadratic recast principle, which makes it possible to avoid the need for iterative processes (there are no convergence problems and no unpredictable computation costs), temporal discretization (it is a frequency domain approach), and the use of numerical schemes in the computation of the derivative (the Jacobian can easily be calculated analytically). The original bubble models are thus transformed into new nonlinear systems (extended state equations), in which the nonlinearities are at most quadratic. The application of the harmonic balance method to quadratic models is recognized at once even if one is searching for solutions to problems involving large numbers of harmonics.

In order to give an explicit picture of the transformation procedure, we will start by presenting the method used to recast the nonlinear system in order to have at most quadratic polynomial nonlinearities. For this purpose, we take the simple case of the forced Duffing oscillator [39]. This simple model corresponds fairly closely to the free bubble radial oscillations in a viscous fluid described by Lauterborn.

2. Generic model: the forced Duffing oscillator

The normalized forced Duffing oscillator is described by the following non-autonomous equation:

$$\ddot{u} + 2\mu\dot{u} + u + \alpha u^3 = f\cos(\lambda t). \tag{1}$$

In this model, the damping coefficient μ, the degree of nonlinearity α and the force amplitude f are constant; the forcing angular frequency is taken to be the varying parameter λ. By taking $v(t) = \dot{u}(t)$ and $\varpi(t) = u^2(t)$, this equation can be recast in quadratic form:

$$\begin{cases} \underbrace{\dot{u}}_{} & = & & \underbrace{v}_{} \\ \underbrace{\dot{v}}_{} & = & \underbrace{f\cos(\lambda t)}_{} & \underbrace{-2\mu v - u}_{} & \underbrace{-\alpha u\varphi}_{} \\ \underbrace{0}_{m(\dot{\mathbf{z}})} & = & \underbrace{0}_{c(t,\lambda)} & \underbrace{\varpi}_{l(\mathbf{z})} & \underbrace{-uu}_{q(\mathbf{z},\mathbf{z})} \end{cases}, \tag{2}$$

where $\mathbf{z} = [u, v, \varpi]^t$, and the forcing term is written in terms of c. The forcing angular frequency is related to the response frequency by taking $\omega = k\lambda$ (where k is an integer). In the Harmonic Balance Method, the term $u(t)$ is expanded into harmonics with respect to ω. The compact expression for the equivalent quadratic system is therefore

$$m(\dot{\mathbf{z}}) = c + l(\mathbf{z}) + q(\mathbf{z}, \mathbf{z}). \tag{3}$$

The unknown vector $\mathbf{z}$ (size N_e) contains the original components u and v plus the auxiliary variable ϖ added to transform (1) into the quadratic form (2). The right-hand side of (2) comprises vector c, which is independent of $\mathbf{z}$; m and l are linear operators acting on $\mathbf{z}$; q is a quadratic vector operator that is linear with respect to both inputs.

The harmonic balance method consists in searching for periodic solutions to Eq. (2): these solutions are expressed as truncated Fourier series:

$$\mathbf{z}(t) \approx \mathbf{z}_0 + \sum_{k=1}^{H} (\mathbf{a}_k \cos k\lambda t + \mathbf{b}_k \sin k\lambda t). \tag{4}$$

Substituting this expression into system (2) and balancing the terms corresponding to the frequency components $((\mathbf{a}_k, \mathbf{b}_k), 1 \leq k \leq H)$ give a system of $(2H+1) \times N_e$ algebraic equations for $(2H+1) \times N_e + 1$ unknowns: the $(2H+1) \times N_e$ components of vector $\mathbf{z}$ and angular frequency λ. The branches of solutions of this algebraic system are then followed using a dedicated continuation (ANM) method, which can be used to solve nonlinear algebraic systems of the form

$$\mathbf{G}(\mathbf{U}, \lambda) = 0. \tag{5}$$

Here, $\mathbf{G}$ and $\mathbf{U}$ have the same dimension $N = (2H+1) \times N_e$. The ANM principle consists in following (approximating) branches of solutions assumed to be power series of the pseudo-arclength path parameter s. Let $\mathbf{x}(s) = (\mathbf{U}(s), \lambda(s))$ be the current branch, $\mathbf{x}_0$ be a regular solution and $\dot{\mathbf{x}}_0 = (d\mathbf{x}/ds)(\mathbf{x}_0)$ be the tangent. By projecting this solution onto $\dot{\mathbf{x}}_0$, the pseudo-arclength parameter s can be defined as

$$ds = d\mathbf{x}^T \cdot \dot{\mathbf{x}}_0. \tag{6}$$

A section of the branch crossing $\mathbf{x}_0$ is found using the following development:

$$\begin{cases} \mathbf{U}_{p_{max}}(s) = \mathbf{U}_0 + \sum_{p=1}^{p_{max}} s^p \mathbf{U}_{0,p}, \\ \lambda_{p_{max}}(s) = \lambda_0 + \sum_{p=1}^{p_{max}} s^p \lambda_{0,p}, \end{cases} \tag{7}$$

where p_{max} is an arbitrary integer ($p_{max} = 30$ in Manlab). Then, in the neighborhood of $\mathbf{x}_0$, a Taylor series expansion of $\mathbf{G}$, i.e., a power series of the pseudo-path parameter s, yields p_{max} systems of $N+1$ linear equations. The length of this part of the branch (the section) is calculated *a posteriori* using a user-defined parameter ε:

$$\forall s \in [0, s_{max}], \quad |\mathbf{G}(\mathbf{U}(s), \lambda(s))| < \varepsilon. \tag{8}$$

This approach has two advantages: first, the computational cost of the series is low since all the linear systems to be solved have the same Jacobian matrix. Second, the lengths of the sections are given by the values of s_{max}: no step-length strategy is therefore required and the continuation algorithm is very robust.

This procedure yields only approximate solutions, since in expansion (4), no harmonic terms greater than H are included. However, if the number of harmonics H is large enough, accurate solutions can be obtained.

Fig. 1 shows the frequency–amplitude diagram of the response obtained in the case of a "hardening" system ($\alpha \geq 0$). A classical bent resonance curve as well as some additional peaks corresponding to superharmonic resonances can be observed. Note that only the individual amplitudes $A_i = \sqrt{a_{u,i}^2 + b_{u,i}^2}$ of the odd harmonics have been plotted, since the even harmonics ($A_0, A_2, A_4, \ldots$) are equal to zero. The frequency responses of "softening" systems ($\alpha \leq 0$) are shown in Figs. 2 and 3, where instabilities and the so-called *jump-frequencies* can be observed. As we will see below, bubbles and contrast agents are mainly softening systems. At the jump-down (respectively, the jump-up) frequency, the vibration amplitude of the system suddenly decreases (paths [3]–[4] on the curves) (respectively increases (paths [3']–[2])) when it
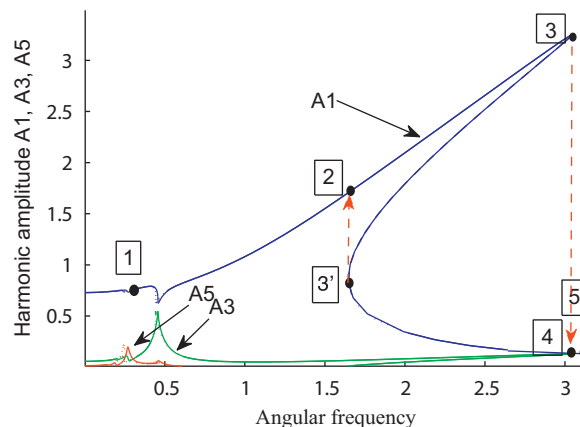

Fig. 1. Duffing oscillator, Eq. (1) where $\mu = 0.05$, $f = 1.0$ and $\alpha = 1$ (a "hardening" system), as in [55]. This figure shows the amplitude of harmonics 1, 3 and 5 versus the forcing angular frequency λ. Continuous line: results obtained when 5 harmonics are included ($H=5$ in Eq. (4)). Dotted line: results obtained when 9 harmonics are included.
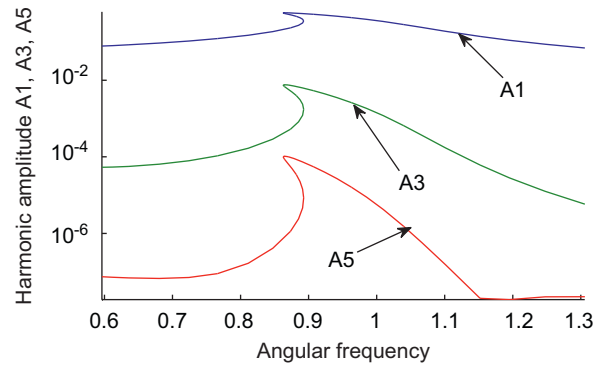
Fig. 2. Duffing oscillator (log scale), Eq. (1) where $\mu = 0.05$, $\alpha = -0.5$ ("softening" system) and $f = 0.05$. Amplitude of harmonics 1, 3 and 5 versus the forcing angular frequency λ.
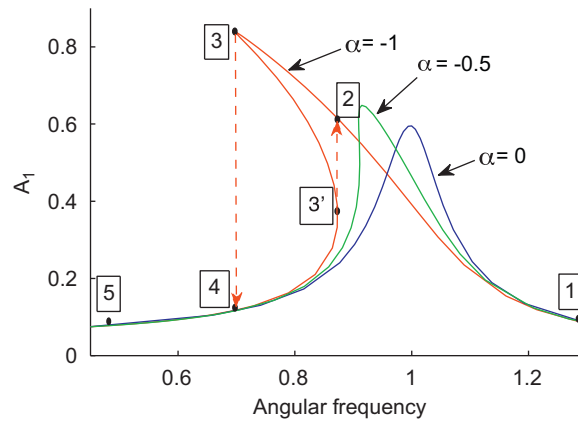

Fig. 3. Duffing oscillator, Eq. (1) where $\mu = 0.05$ and $f = 0.04$. A_1 amplitudes versus the angular frequency when $\alpha = -1$, -0.5 and 0 (softening systems).

is excited harmonically with a slowly increasing (respectively decreasing) frequency. The frequencies at which these jumps occur depend on whether the modulation is increasing or decreasing and whether the nonlinearity has hardening (Fig. 1) or softening (Fig. 2) effects.

Besides, assuming the presence of a harmonic balance restricted to the fundamental component, the jump-down frequency of the Duffing oscillator can be written as [54]

$$\omega_J \approx \frac{1}{2^{1/2}} \left(1 + \left[1 + \frac{3\alpha}{4\mu^2} \right]^{1/2} \right)^{1/2} \tag{9}$$

and the vibration amplitude at this frequency is given by

$$A_J \approx \left(\frac{2}{3\alpha} \left(\left[1 + \frac{3\alpha}{4\mu^2} \right]^{1/2} - 1 \right) \right)^{1/2}. \tag{10}$$

For ω_J to be real in a softening system ($\alpha < 0$), the following condition is necessary:

$$\alpha \geq \alpha_J = -4\mu^2 / 3. \tag{11}$$

If this condition is not met, no jump-down will occur.

In addition, if the assumption $3\alpha/(4\mu^2) \ll 1$ is valid (this is quite restrictive if there is little damping), the jump-down frequency can be written as $\omega_J \approx 1 + 3\alpha/32\mu^2$ and the amplitude at the jump-down frequency is given by $A_J \approx 1/2\mu$. The degree of nonlinearity alone is therefore not the main parameter here but how it compares with the damping, i.e., the ratio $3\alpha/4\mu^2$ is the relevant parameter.

In a first-order approximation, the overall amplitude of the response of the system therefore depends mainly on the damping, and the deviation of the jump-down frequency from the natural frequency of the associated linear system (measurements obtained with a low-level excitation force) depends on the degree of nonlinearity and on the damping via the ratio $3\alpha/4\mu^2$.

To sum up, the key idea on which this procedure is based is quadratic recast. It provides a closed form solution to the continuation problem in the frequency domain with an arbitrarily large number of harmonics [39]. In addition, neither iterative processes nor temporal sampling methods are required, and low convergence and possible aliasing problems are thus avoided. The Duffing model introduced here serves as a pedagogical introduction to the HBM method based on the use of the Manlab software program. This model is fairly representative of the various theoretical models for free and encapsulated bubbles in viscous fluids that will now be analyzed.

3. Bubble in a viscous fluid

3.1. The "RPNNP" model

Let R be the radius of the vibrating bubble and R_0 be the radius at rest. The "RPNNP" equation is

$$\rho_L\left[R\ddot{R}+\frac{3}{2}\dot{R}^2\right]=\left(P_0+\frac{2\sigma}{R_0}\right)\left(\frac{R_0}{R}\right)^{3\zeta}-\frac{2\sigma}{R}-4\eta_L\frac{\dot{R}}{R}-P_0+P\cos\Omega t, \tag{12}$$

where P_0 is the static pressure in the fluid, ρ_L is the fluid density, σ is the surface tension, η_L is the fluid viscosity, Ω is the angular frequency of the plane pressure-wave and ζ is the polytropic exponent.

In order to be able to recast this expression in quadratic form, we take isothermal oscillations: $\zeta=1$. This working hypothesis obviously does not correspond very closely to reality but it lends itself to the numerical limitations of the present Manlab® software program, in which no differentiation of the non-integer order has yet been implemented.

We write $\tau=\omega t$ and $dX/d\tau=\dot{X}$. Taking $u=R/R_0$, $v=\dot{R}/R_0$, $x=1/u$, $y=x^2$, $z=v^2$ and $f=P\cos\Omega t$, Eq. (12) can be rewritten as

$$\dot{v}=-\frac{P_0}{\rho_L\omega^2R_0^2}x-\frac{2\sigma/R_0}{\rho_L\omega^2R_0^2}y+\frac{P_0+2\sigma/R_0}{\rho_L\omega^2R_0^2}y^2-\frac{4\eta_L}{\rho_L\omega R_0^2}yv-\frac{3}{2}xz+\frac{1}{\rho_L\omega^2R_0^2}xf, \tag{13}$$

where the respective coefficients are

$$A=\frac{P_0}{\rho_L\omega^2R_0^2},\quad B=\frac{2\sigma/R_0}{\rho_L\omega^2R_0^2},\quad C=\frac{4\eta_L}{\rho_L\omega R_0^2}\quad\text{and}\quad D=\frac{1}{\rho_L\omega^2R_0^2}, \tag{14}$$

and $P_0=1.013\times10^5$ Pa, $\rho_L=10^3$ kg/m³, $\sigma=72\times10^{-3}$ N/m, $\eta_L=10^{-3}$ Pa s, $\omega=10^6$ rad/s, $R_0=2\times10^{-6}$ m (air bubble in water of a micrometric size studied in the megahertz range). Eq. (13) can take the form of a quadratic system, giving the following state space extension of vector $\mathbf{z}$:

$$\begin{cases}\dot{u} & = & & v \\ \dot{v} & = & & -Ax-By & +(A+B)y^2-Cyv-\dfrac{3}{2}xz+Dxf \\ 0 & = & 1 & & -ux \\ 0 & = & & y & -x^2 \\ 0 & = & & z & -v^2 \\ \underbrace{0}_{m(\dot{Z})} & = & \underbrace{-P\cos(\Omega t)}_{c(t)} & \underbrace{f}_{l(Z)} & \underbrace{}_{q(Z,Z)}\end{cases}, \tag{15}$$

where the space vector is $\mathbf{z}=[u,v,x,y,z,f]$.

It can be observed here that the compact expression for the equivalent quadratic system is similar to (3). The unknown vector $\mathbf{z}$ (size $N_e=5+1$) contains the original components u, v, plus the auxiliary variables x,y,z,f that have been added to transform (12) into the quadratic form (15).

Since vector $\mathbf{z}$ was written in the general form (4),

$$u=\frac{R}{R_0}=u_0+\sum_{k=1}^{H}(a_{u,k}\cos k\Omega t+b_{u,k}\sin k\Omega t). \tag{16}$$

When the amplitude of the driving term is very low ($P\simeq0.01$ Pa) in comparison with the other terms in Eq. (12), the graph of amplitude A_1 versus the angular frequency Ω describes the *free* response of the system. At low amplitudes, this amplitude/frequency curve is still tangential to the linear mode, $\Omega_L=\omega_0=8.72\times10^6$ rad/s (cf. Table 1), and then gradually bends to the left with the activation intensity: this corresponds to a "softening" system such as that depicted in Figs. 2 and 3.

Note: In all the following figures, the angular frequency unit is 10^6 rad/s.

Changing radius R_0 of the bubble or taking the surface tension $\sigma=72\times10^{-3}$ N/m does not alter the overall shape of the amplitude/angular frequency curve.

Only the "starting" angular frequency Ω_L at which the amplitude is non-zero changes. This value is the undamped natural frequency of the linear system (the nonlinear term set to zero) associated with Eq. (12): i.e., the Minnaert

Table 1
Linear angular frequency without taking the surface tension into account (Minnaert) and taking this parameter into account (Robinson).

	Radius R_0 (µm)					
	1	2	3	5	10	17
ω_{Minnaert} (10^6 rad/s)	17.43	8.72	5.81	3.49	1.74	1.025
ω_{Robinson} (10^6 rad/s)	24.33	10.58	6.66	3.80	1.82	1.05
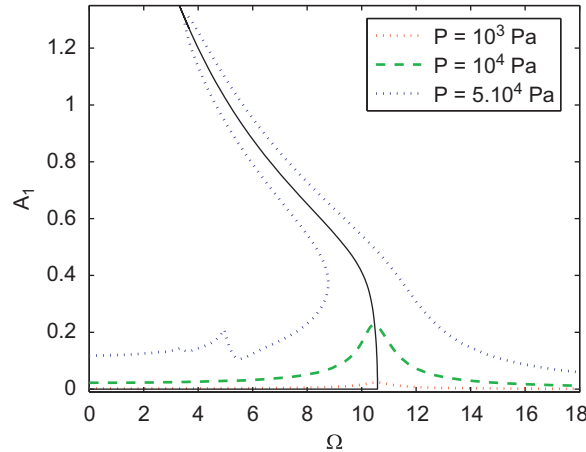
Fig. 4. Frequency responses of the damped system (broken lines) and those of the undamped system (continuous line).

isothermal angular frequency when $\sigma = 0$ or the Robinson and Buchanan [56] angular frequency when the surface tension is taken into consideration.

The angular frequencies obtained with these two models expressed as functions of the radius are presented in Table 1; these values fit the results obtained with the Manlab software program very closely; we systematically obtain $\Omega_L = \omega_{\text{Minnaert}}$ (respectively, $\Omega_L = \omega_{\text{Robinson}}$; $\sigma \neq 0$) when $A_1 = 10^{-3}$.

Introducing the fluid viscosity (in the case of water, $\eta_L = 10^{-3}$ Pa s) into the model leads to changing the resonance behavior of the bubble. In order to observe this resonance behavior, since the damping term is non-negligible here in comparison with the other parameters featuring in the equation, it is necessary to increase the amplitude P of the driving oscillator. In fact we can observe (cf. Fig. 4) the main resonance of the forced system which occurs when the angular frequency of the driving harmonic component approaches that of the free system (in this case, $R_0 = 2$ µm, $\omega_0 = 10.57 \times 10^6$ rad/s), which corresponds to the angular frequency given by Houghton [57]:

$$\omega_{\text{Houghton}} = \frac{1}{R_0} \sqrt{\frac{3\gamma\left(P_0 + \frac{2\sigma}{R_0}\right) - \frac{2\sigma}{R_0}}{\rho_L} - \frac{4\eta_L^2}{\rho_L^2 R_0^2}}.$$

(17)

Fig. 5 shows the evolution of the first, second and third harmonics versus the angular frequency, where the amplitude of the driving source is $P = 5 \times 10^4$ Pa. The main resonance is given when $\Omega = \omega_0$, but secondary resonances, called super-harmonics, also occur when the angular activation frequency equals $\omega_0/2$ or $\omega_0/3$. At this secondary resonance, the amplitude of the second harmonic becomes larger than that of the first one (the fundamental). This has been found to be a useful means [58] of transmitting ultrasonic waves at the angular frequency $\Omega = \omega_0/2$ with a sufficiently large amplitude ($P \geq 50$ kPa = 0.5 atm) in order to perform nonlinear (harmonic) imaging of a bubble in water or in tissues. However, when the amplitude of the driving wave is less than 10 kPa = 0.1 atm, the nonlinear character of the bubble response is "erased" (in water) by the viscous attenuation. A linear damped oscillator model may suffice in this case to characterize the bubble.

The frequency response curves obtained here obviously resemble those defined by the damped Duffing oscillator. The Duffing model can therefore serve as a "canonical" model for the "free bubble in a viscous fluid system" and to characterize this system with the following pair of parameters: the damping and the degree of nonlinearity.

If we take an isolated bubble in a viscous fluid, a numerical experiment can be performed (using the Matlab "ODE45" solver) in which the excitation amplitude is held constant but the frequency is varied continuously and linearly. Then, as described in the previous section, the occurrence of jumps in the amplitude response will be observed.

If, for instance, the excitation is applied at a higher frequency than the natural linear frequency, a decreasing frequency sweep will induce a larger jump in the amplitude than an increasing frequency sweep starting at a lower frequency than
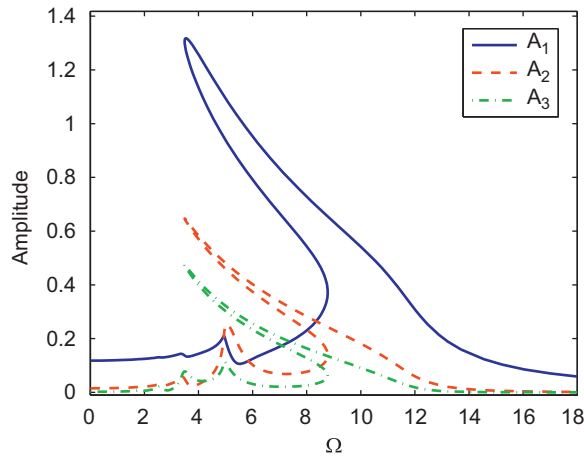
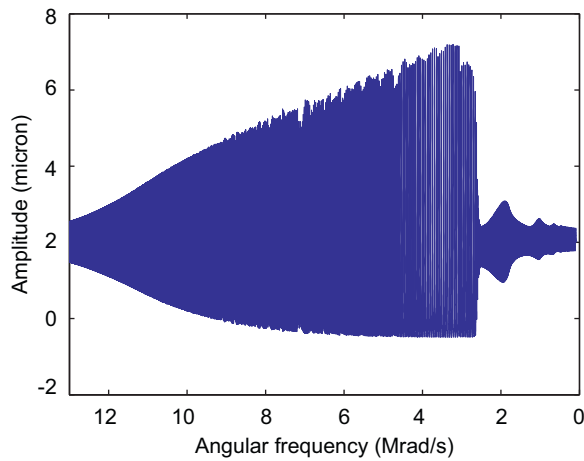**Fig. 5.** Amplitude of the first, second and third harmonics—$P = 5 \times 10^4$ Pa.

Fig. 6. Time response of a 4-μm bubble to a linear down-chirp (range [2.1, 0] MHz) with a constant amplitude (50 kPa).
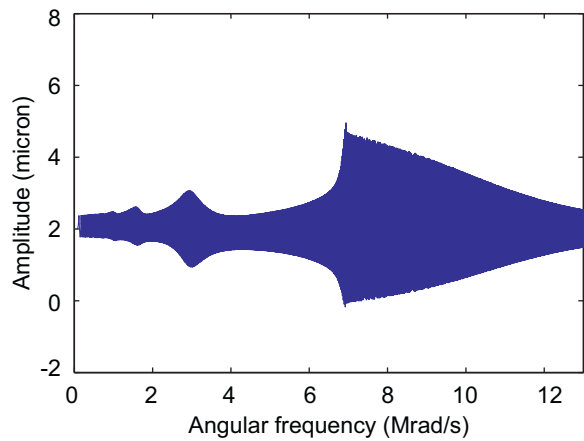

Fig. 7. Time response of a 4-μm bubble to a linear up-chirp (range [0, 2.1] MHz) with a constant amplitude (50 kPa).

the natural frequency (cf. Fig. 6 versus Fig. 7). In practice, this means that a higher signal to noise ratio will be obtained in the former case. In addition, this distinction between the increasing and the decreasing sweeps could serve as the basis of a *differential harmonic imaging* procedure for detecting the presence of the bubbles.

3.2. Dissipative effects of sound radiation

The radial pulsations of a bubble are affected by three damping mechanisms which are of some importance when estimating the nonlinear behavior of the bubble. These effects are losses due to viscous processes occurring at the bubble wall and to the thermal conduction and energy dissipation resulting from acoustic radiation. Although the first two effects are included in the Rayleigh–Plesset (RPNNP) model (Eq. (12)), the dissipative processes due to the radiation of spherical sound waves are not. A corrective term, which has been found to be a reliable index to these losses, is therefore generally added [41,53], and the corresponding equation will now be studied.

As far as thermal losses are concerned, the polytropic nature of the gas compression induces hysteresis effects. Because of the isothermal limitations of the Manlab software program, the net flow of heat into the liquid is necessarily null during a pulsation cycle, and thermal damping cannot be taken into account in the present study.

The modified RPNNP model accounting for radiation damping can be written as [53,59]

$$\rho_L\left[R\ddot{R}+\frac{3}{2}\dot{R}^2\right]=p_B(t)-P_0+P\cos\Omega t+\frac{R}{c}\left(1-\frac{\dot{R}}{c}\right)\frac{dp_B}{dt},\tag{18}$$

where $p_B(t)$ is the pressure exerted on the liquid due to the pulsation of the bubble,

$$p_B(t)=\left(P_0+\frac{2\sigma}{R_0}\right)\left(\frac{R_0}{R}\right)^{3\zeta}-\frac{2\sigma}{R}-4\eta_L\frac{\dot{R}}{R}.\tag{19}$$

Substituting $p_B(t)$ into Eq. (20) gives the first-order approximation:

$$\rho_L\left[R\ddot{R}+\frac{3}{2}\dot{R}^2\right]=\left(P_0+\frac{2\sigma}{R_0}\right)\left(\frac{R_0}{R}\right)^{3\zeta}\left[1-3\zeta\frac{\dot{R}}{c}\right]-\frac{2\sigma}{R}\left[1-\frac{\dot{R}}{c}\right]-4\eta_L\frac{\dot{R}}{R}-P_0+P\cos\Omega t.\tag{20}$$

Once again, the behavior is assumed to be isothermal ($\zeta=1$) because of the present numerical possibilities of the Manlab software program.

Quadratic form recast: Eqs. (12) and (20) differ in the presence of the terms $\dot{R}/c$ on the right-hand side. In order to derive the associated quadratic form of Eq. (20), we re-use the variables defined in the above algebraic system (15), to which one supplementary variable $\alpha=y^2$ and two supplementary constants $E=(A+B)(3\Omega R_0/c)$ and $F=B\Omega R_0/c$ are added.

Eq. (20) is therefore equivalent to the following system of first-order differential equations:

$$\begin{cases} u' & = & & v \\ v' & = & & -Ax-By+(A+B)\alpha & -Cvy-\frac{3}{2}xz+Dxf-E\alpha v+Fyv \\ 0 & = & 1 & & -xu \\ 0 & = & & y & -x^2 \\ 0 & = & & z & -v^2 \\ 0 & = & -P\cos\Omega t & +f \\ 0 & = & & \alpha & -y^2 \end{cases},\tag{21}$$

where $\mathbf{z}=[u,v,x,y,z,f,\alpha]^t$. Once again, the operators in the formal expression

$$m(\dot{\mathbf{z}})=c(t)+l(\mathbf{z})+q(\mathbf{z},\mathbf{z})\tag{22}$$

can be easily identified in the above system.

In Fig. 8, the effects of radiation damping are clearly shown by the level of erosion undergone by the bending: it can be seen here that the peak amplitude decreases only slightly when a linear up-chirp is applied (almost no differences observed between damped and undamped responses) and the peak amplitude decreases significantly when the bubble is activated by a linear down-chirp (strong differences observed between the two responses).

4. Shelled contrast agent

Most contrast agent bubbles are encapsulated in a shell that has two main effects on the acoustic response. First, the shell renders the bubble stiffer than a free gas bubble of the same size, making its resonance frequency greater than that of the free bubble and reducing the nonlinear effects. Second, since the shell makes the bubble more viscous, the sound energy absorbed is converted into heat instead of being radiated; the scattering/attenuation ratio therefore decreases. Many authors have concluded that the influence of the shell is crucial and have confirmed that the properties of the acoustic field scattered by the agent are strongly dependent on the shell properties. Various shell models have been proposed: Fox and Hertzfeld [60] studied bubbles in sea water and underlined the influence of the organic shell; De Jong et al. [17,18] developed empirical models for Albunex; Church published a well-founded visco-elastic model [19] involving linear material properties but also including nonlinear geometric effects; and Angelsen et al. [20] and Hoff et al. [21] proposed an exponential stress strain relationship for the shell material. A few years back, Marmottant introduced a "buckling" model [23] accounting for buckling and rupture processes. The last two models will be analyzed here, but as we
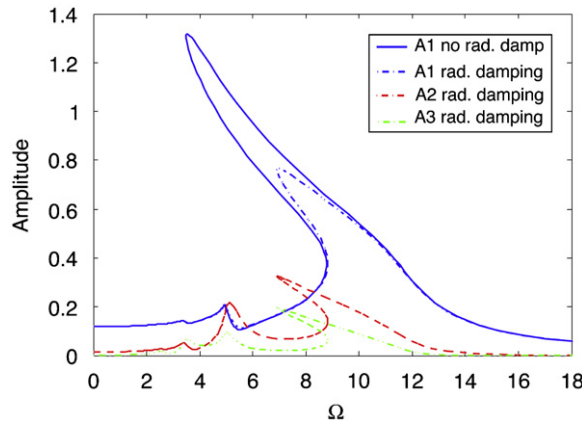
Fig. 8. Radiation damping effects: amplitude of the first, second and third harmonics—$P = 5 \times 10^4$ Pa.

will focus on the physical trends associated with the shell mechanics, radiation damping will not be dealt with in the following two paragraphs.

4.1. The polymer-shell contrast agent—Hoff model

Hoff modeled contrast agents assuming the existence of a low shell thickness, e_s, in comparison with the internal and external radii, i.e. $e_s \ll R_1, R_2$. This assumption makes it possible to reduce the equation for the movement. Taking R_2 to denote the external radius of the shell and writing $R = R_2$, the equation reduces to

$$\rho_L \left[R\ddot{R} + \frac{3}{2}\dot{R}^2 \right] = \left(P_0 + \frac{2\sigma}{R_0} \right) \left(\frac{R_0}{R} \right)^{3\zeta} - \frac{2\sigma}{R} - 4\eta_L \frac{\dot{R}}{R} - P_0 + P\cos\Omega t - 12\eta_S R_0^2 e_S \frac{\dot{R}}{R^4} - 12\mu_S \frac{R_0^2 e_S}{R^3} \left(1 - \frac{R_0}{R} \right), \tag{23}$$

where μ_s and η_s are the shear modulus and the shear viscosity of the shell, respectively, which can be determined by performing ultrasound attenuation measurements. This relation is based on that given by Church in the case of incompressible viscoelastic (Kelvin–Voigt) materials: the constitutive equation determines the radial component of the stress tensor ($R_1 \le r \le R_2$):

$$T_{S,r} = (\lambda_S + 2\mu_S) \cdot \nabla_r \varepsilon_r + 2\lambda_S \frac{\varepsilon_r}{r} + 2\eta_S \nabla_r \dot{R}_1, \tag{24}$$

where λ_S and μ_S are the Lamé constants and ε_r is the shell radial strain.

Quadratic form recast: Eqs. (12) and (23) differ only in the last two terms, which sum up the shell contribution. In order to derive the associated quadratic form of Eq. (23), we use the variables defined in the algebraic system (15), to which the two supplementary variables $\alpha = y^2$ and $\beta = \alpha x$ and the two supplementary constants $E = 12\mu_S e_S / \rho_L \omega^2 R_0^3$ and $F = 12\eta_S e_S / \rho_L \omega R_0^3$ are added.

Eq. (23) is therefore equivalent to the following system:

$$\begin{cases} u' = & v \\ v' = & -Ax - By + (A + B - E)\alpha + E\beta & -Cvy - \frac{3}{2}xz + Dxf - F\beta v \\ 0 = & 1 & -xu \\ 0 = & y & -x^2 \\ 0 = & z & -v^2 \\ 0 = -P\cos\Omega t & +f \\ 0 = & \alpha & -y^2 \\ 0 = & \beta & -\alpha x \end{cases}, \tag{25}$$

where $\mathbf{z} = [u, v, x, y, z, f, \alpha, \beta]^t$.

This model was drawn up by Hoff for characterizing a contrast agent with a gas core and a polymer shell (such as AI-700 manufactured by Acusphere or Sonavist by Shering). Based on the assumption that the shell thickness equals 5 percent of the nominal radius R_0 of the contrast agent, comparisons with the theoretical predictions and experimental data make it possible to assess the viscoelastic coefficients of the shell [21]: $\mu_s = 11.6$ MPa and $\eta_s = 0.48$ Pa s.

Results: First, in order to assess the influence of the shear modulus μ_s component of the UCA response, the shear viscosity is set at zero. Fig. 9 shows the evolution of the fundamental amplitudes A_1 of four UCAs (radius $R_0 = 3$ μm) with shear modulus values of 11.6, 50, 88 and 150 MPa (these values are based on [19]). Increasing μ_s values correspond to increasing shell rigidity, which restricts the amplitude of the oscillations and reduces the nonlinearity of the UCA
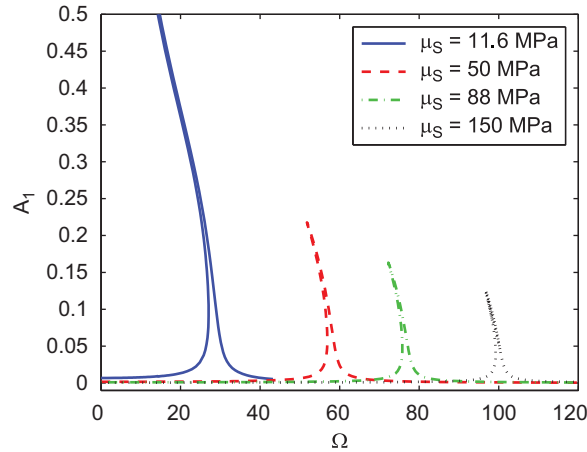
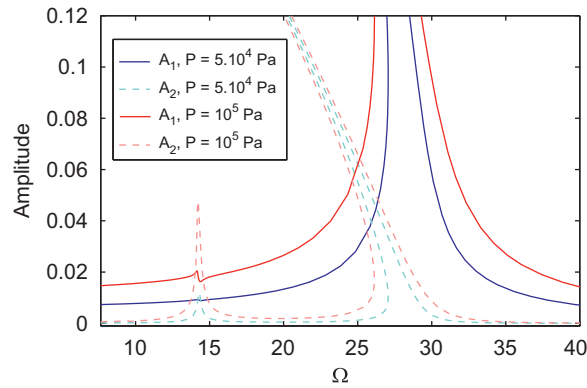**Fig. 9.** Influence of the shear modulus on the amplitude A_1 of the fundamental component.

Fig. 10. Zoom showing the amplitude of the first and second harmonics ($\mu_s = 11.6$ MPa).

responses. The values of the angular frequencies at which the amplitudes start to increase are completely in agreement with those predicted by the closed-form expression obtained by linearizing equation (23) [21].

The first and second harmonic amplitude values are illustrated in Fig. 10 at a given shear modulus value ($\mu_s = 11.6$ MPa) at two excitation levels ($P = 5 \times 10^4$ Pa, i.e. 0.5 atm and $P = 10^5$ Pa, i.e. 1 atm). The main resonance greatly exceeds the secondary super-harmonic resonance. However, since in the latter case, the secondary harmonic amplitude is greater than the fundamental one when the amplitude of the driving source is large enough (typically, of the order of 100 kPa), the secondary resonance is still of interest for nonlinear tissue contrast imaging purposes. Besides, at a given shear modulus ($\mu_s = 11.6$ MPa, for instance), the viscosity of the shell greatly reduces the oscillation amplitudes, as shown in Fig. 11. The resonance is almost absent at viscosity values such as $\eta_s = 0.48$ Pa s, which is in agreement with Hoff's conclusion. Since the experimental measurements [21] were performed on polydisperse UCA populations, the fact that multiple scattering was not taken into account and the assumption that the properties (thickness, visco-elasticity) are constant suggest that in this case, the shell viscosity was certainly over-estimated.

4.2. Phospholipid-coated contrast agent: the Marmottant model

In this case, we are interested in characterizing a lipid-shell UCA (e.g. Sonovue manufactured by Bracco, or Imagent by Alliance): the model given in [23] corresponds to the following ordinary differential equation:

$$\rho_L \left[R\ddot{R} + \frac{3}{2}\dot{R}^2 \right] = \left(P_0 + \frac{2\sigma(R_0)}{R_0} \right) \left(\frac{R_0}{R} \right)^{3\zeta} - \frac{2\sigma(R)}{R} - 4\eta_L \frac{\dot{R}}{R} - 4\kappa_S \frac{\dot{R}}{R^2} - P_0 + P\cos \Omega t, \tag{26}$$

where κ_S denotes the surface dilatational viscosity of the phospholipid monolayer coating. In the linear regime, the changes in the surface tension with the area A can be expressed using the elastic compression modulus χ_S defined by $\chi_S = A(\mathrm{d}\sigma/\mathrm{d}A)$. In this regime, where no buckling and rupture of the monolayer occur, the surface tension is a linear
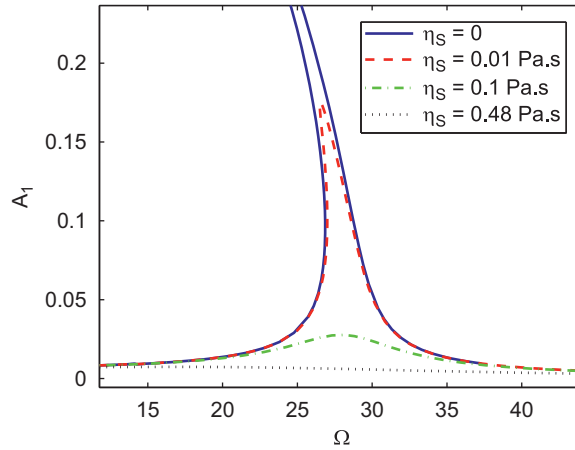
Fig. 11. Influence of the viscosity of the shell on the amplitude A_1.

function of the area, or of the square of the radius:

$$\sigma(R) = \chi_S \left(\frac{R^2}{R_b^2} - 1 \right), \tag{27}$$

where R_b is the threshold radius at which buckling of the phospholipid molecules occurs.

Quadratic form recast: Let us take $g = xy$, $\mathbf{z} = [u, v, x, y, z, f, g]^t$ (variables u, v, x, y, z and f remain unchanged) and let us define the following constants:

$$A_M = \frac{2\chi_S}{\rho_L \omega^2 R_0 R_b^2}, \quad B_M = \frac{P_0}{\rho_L \omega^2 R_0^2}, \quad C_M = \frac{2\chi_S}{\rho_L \omega^2 R_0^3}, \quad D_M = \frac{R_0^2}{R_b^2} - 1,$$

$$E_M = \frac{4\eta_L}{\rho_L \omega R_0^2}, \quad F_M = \frac{4\kappa_S}{\rho_L \omega R_0^3}, \quad G_M = \frac{1}{\rho_L \omega^2 R_0^2}. \tag{28}$$

Eq. (26) can be rewritten in the quadratic form:

$$\begin{cases} u' &= & v \\ v' &= & -A_M & -B_M x + C_M y & -\dfrac{3}{2}xz + (B_M + C_M D_M)y^2 - E_M vy - F_M gv + G_M xf \\ 0 &= & 1 & -xu \\ 0 &= & y & -x^2 \\ 0 &= & z & -v^2 \\ 0 &= & -P\cos\Omega t & +f \\ 0 &= & g & -xy \end{cases}, \tag{29}$$

Fig. 12 shows the natural ($P = 10^{-2}$ Pa) response of the undamped system ($R_0 = R_f = 1.98\,\mu m$, $\chi_S = 0.55\,N/m$ and $\eta_L = \kappa_S = 0$) as well as the forced response ($P = 5 \times 10^4$ Pa) of the damped system, taking only the liquid viscosity into account ($\eta_L = 10^3$ Pa s). The shell viscosity is also examined ($\kappa_S = 7.2 \times 10^{-9}$ N). The values of these parameters were based on [23,25].

It can be seen from Fig. 12 that the system hardens at the lower activation amplitudes before softening as the driving power increases. However, once again, taking the viscosity of both fluid and shell into account drastically reduces the oscillation amplitude and abolishes the nonlinearity of the contrast agent's behavior. This result is in agreement with findings by Van der Meer et al. [25], who established that a simple oscillator model obtained by linearizing the Marmottant model suffices to describe the radial oscillations of a UCA in response to a 40-kPa excitation amplitude. These conclusions were based on experimental data obtained using the Brandaris ultra-fast video camera [25].

Fig. 13 shows the evolution of the first and second harmonics depending on the angular frequency Ω at various driving source amplitude levels P. One can easily spot (on the A_2 curve) the resonances occurring at $\Omega = \Omega_L/2$ and at $\Omega = \Omega_L/3$ when the source amplitude is greater than 100 kPa. It is worth noting that with both of the above models (at similar values of P), at the secondary super-harmonic resonance ($\Omega = \Omega_L/2$), the amplitude of the second harmonic is lower than that of the fundamental. However, here, at the super-harmonic resonance recorded at the highest pressure level, the amplitude of the second harmonic exceeds the main resonance value; this situation has never been encountered so far.
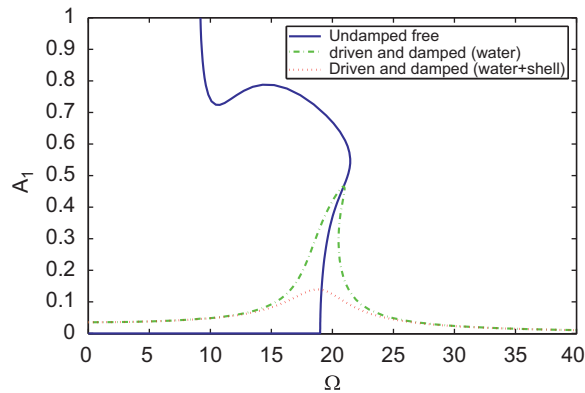
Fig. 12. Marmottant model: influence of the liquid and shell viscosities on the amplitude A_1.
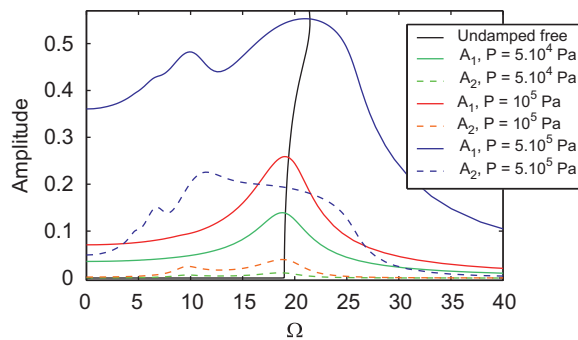

Fig. 13. Effects of the excitation pressure on the first and second harmonics.

5. Application to "small" bubble sizing

The problem of detecting and sizing microbubbles in their host environment has received considerable attention during the last 30 years. In studies using only reflection measurements, most of the methods used have been based on the use of a "pumping" field [3–6,35,59,61–65], the frequency of which is approximately equal to the resonance frequency of the bubble to be detected, associated with an "imaging" field with a higher frequency. When interacting nonlinearly with the bubble, the two waves generate among all the sideband components sum and difference frequencies unambiguously showing spectral peaks depending on the bubble radius. This robust double frequency method has mainly been applied in two ways, depending on the possibility of synchronizing the pump and the imaging fields. Applications with no temporal dependence between these two fields were first introduced. An improved version giving both lateral and axial resolutions was then obtained using a pulsed Doppler approach [4]. A method involving a low frequency "manipulation" pulse altering the scattering properties of the bubble and a phase-controlled high-frequency imaging pulse recently made it possible to generate bubble detection signals [66]. However, when the aim is to detect small bubbles (with diameters ranging between $[1,10]\,\mu m$), in order to prevent decompression sickness and to obtain accurate assessments of the bubble distribution using current medical ultrasound equipment (frequency range [1, 15 MHz]), the double frequency method is no longer practical: with these bubble sizes, the low frequencies required, ranging from 0.65 to 6.5 MHz, coincide with the frequency range of the imaging field, and the relevant sideband components lie beyond the bandpass of the imaging transducers.

It is now proposed to use the nonlinear frequency bubble responses (under the same conditions as in Section 3.2, including radiation damping, Eq. (20)) in order to obtain a small microbubble-detecting/sizing tool. It can be seen from Figs. 14 and 15, which show the frequency responses of air bubbles in water (with the same physical parameters as in Section 3) ranging between 1 and 10 μm in size, that bubbles with a diameter of more than 2 μm show strong nonlinearities when excited by an acoustical pressure wave of 50 kPa. But this is not so in the case of bubbles with radii of less than 1 μm. However, as shown in Fig. 16, increasing the pressure exerted on a 2-μm diameter bubble twofold to 100 kPa restores the nonlinearity of its frequency response.

The nonlinear behavior induces the presence of jump-up and jump-down frequencies, which are specific features of the bubble's (placed in a given viscous fluid) size. If a bubble of a given size is insonified with linearly modulated chirps of decreasing and increasing frequency sweeps which encompass its jump-up frequency, the response of the bubble will be maximum and non-symmetrical, contrary to what occurs with those whose jump-up frequency is not included in this
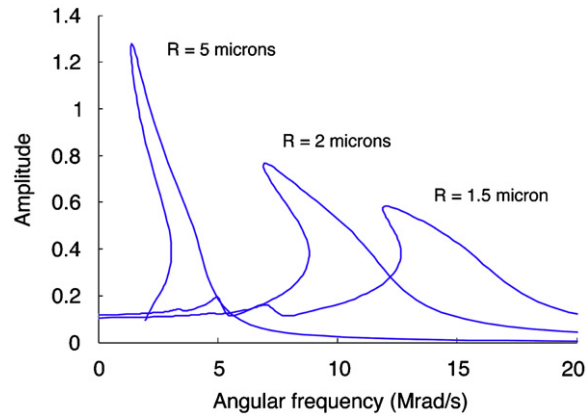
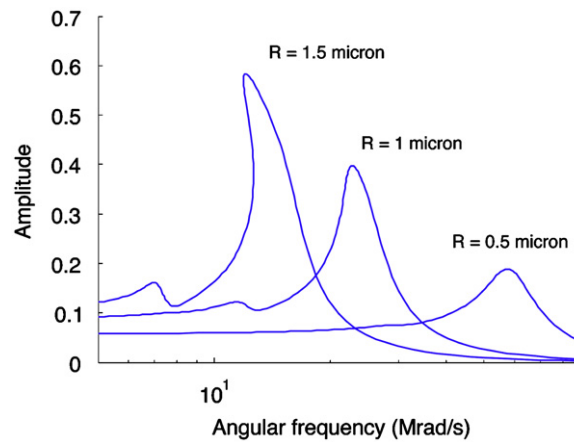**Fig. 14.** Frequency responses of bubbles (diameters 10, 4, 3 μm) to a 50-kPa pressure wave in water.

Fig. 15. Frequency responses (log scale) of bubbles (diameters 3, 2, 1 μm) to a 50-kPa pressure wave in water.
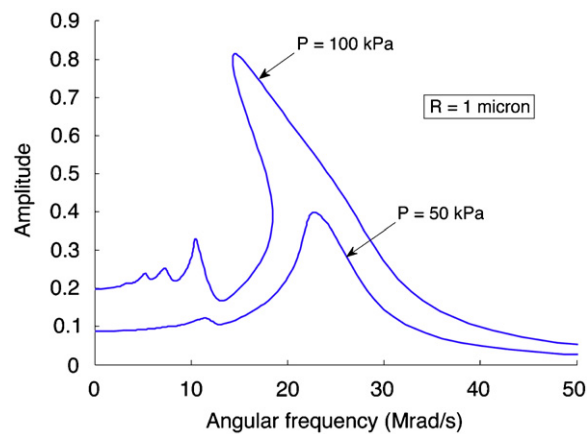

Fig. 16. Frequency responses of a 2-μm diameter bubble to 50-kPa ("linear" behavior) and 100-kPa (nonlinear behavior) pressure waves in water.

interval. For instance, the amplitude signal backscattered by a 4-μm bubble is 2 or 3 times greater than the signals generated by bubbles whose radius differs only by 1 μm. This resonance process is illustrated in Figs. 17–20. In the numerical experiments with various bubble sizes dedicated to the detection of 4-μm bubbles, the 530 μs activation signal is linearly modulated from 1.46 MHz (9.169 Mrad/s) down to 1.41 MHz (8.855 Mrad/s) during the first half of the activation
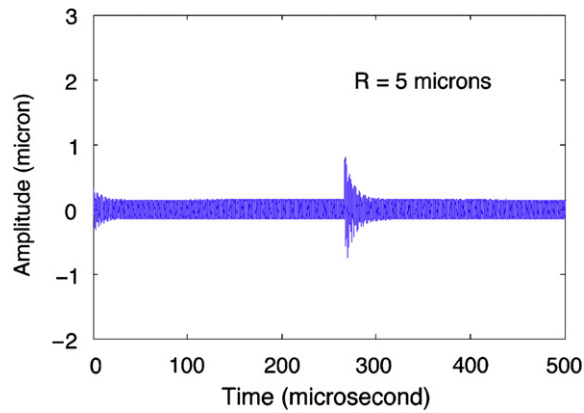
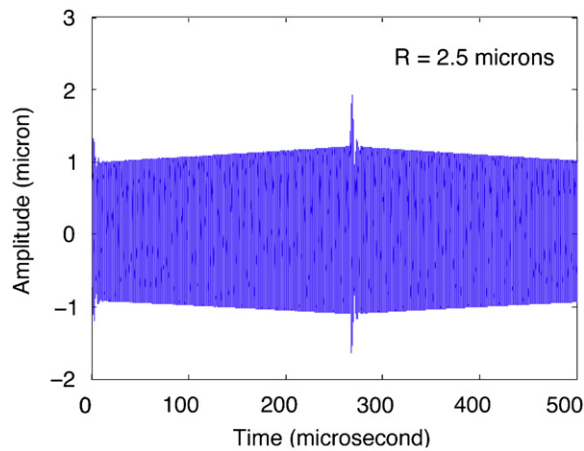Fig. 17. Response of a 10-μm bubble to a linear down/up chirp (range [1.41–1.46 MHz] in water).

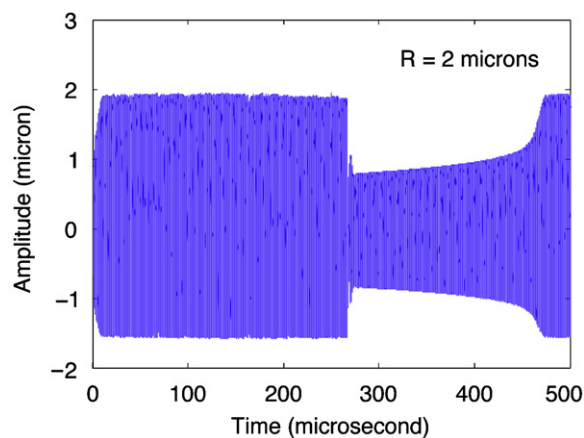Fig. 18. Response of a 5-μm bubble to the same pressure wave as in Fig. 17.

Fig. 19. Response of a 4-μm bubble to the same pressure wave as in Fig. 17.

period before being up-modulated to 1.46 MHz during the second half. The responses of the bubble with time were obtained using the "ODE45" Matlab solver.

The results obtained here show that the temporal responses of the bubbles whose diameters differed by more than 1 μm as compared with the 4-μm reference bubble had symmetrical shapes. This was due to the fact that with these bubbles, the jump-up frequency was not crossed by the frequency sweep. Therefore, only either the upper branch or the
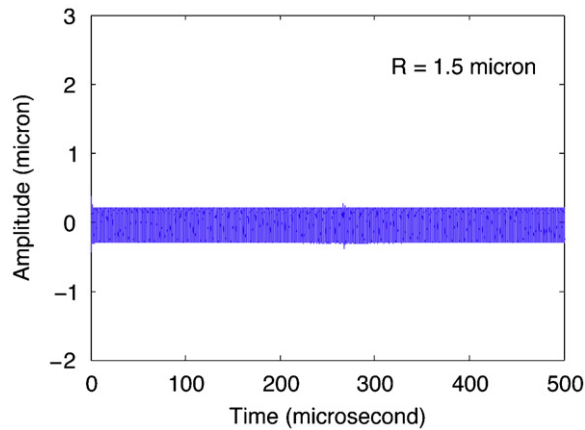
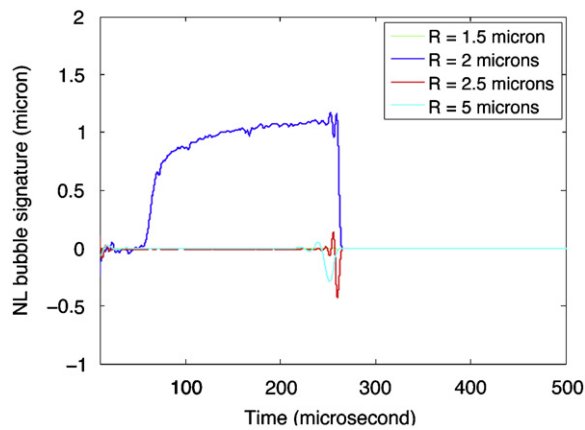Fig. 20. Response of a 3-μm bubble to the same pressure wave as in Fig. 17.

Fig. 21. Nonlinear signatures of various bubbles in response to an activation for 4-μm bubble detection purposes.

lower branch of their frequency response was reversibly followed; however within the resonance zone of the 4-μm bubble, the jump associated with the hysteretic behavior induced an asymmetrical time response. Hence, the idea arose of extracting the signal envelope and calculating the differences between the samples recorded at the same instantaneous frequency, which yields a nonlinear signature for each bubble.

Fig. 21 shows these signatures and proves, for instance, that by applying a simple threshold, it is possible to detect and discriminate between bubbles with diameters in the [1, 10] μm range with a theoretical resolution greater than 1 μm.

6. Conclusion

Methods of characterizing bare and coated (contrast agent) microbubbles are of great interest in many industrial and medical fields. In the search for relevant parameters (precursors) confirming the presence of microbubbles, showing their patterns of size distribution, or yielding an unambiguous picture of their movements (free circulation versus endothelial cell membrane adhesion), finer nonlinear tools and methods are required. This study, which extends previous standard methods of linear analysis to include nonlinear (bubble) behavior, shows that the high order harmonic balance method (HBM) is an efficient method: it provides a simple means, implemented in the Manlab® (open-access software) suite, of investigating the behavior of nonlinear systems such as microbubbles in water. This method was based on the NonLinear Ordinary Differential Equation (NL-ODE) governing the evolution with time of the bubble radius in response to ultrasonic activation. A local periodic solution was obtained which can be "tracked" using a specific continuation technique in conjunction with the HBM. The "manual" pre-processing of the NL-ODE consists in performing a quadratic recast of the nonlinear equations. In the frequency domain, this yields a closed-form solution to the continuation problem with an arbitrary number of harmonics. With this approach, various theoretical models for bubble responses in viscous fluids have been studied, such as the "RPNNP" based model (that can possibly take radiation damping but not thermal damping into

account) for a free microbubble response and the Hoff and Marmottant models, which are dedicated to shelled contrast agents with polymer and phospholipid shells, respectively.

The results obtained using the overall procedure confirm the validity of this method, first by showing that although the number of harmonics included in the computation should not be underestimated, the rapid asymptotic convergence observed means that a fairly satisfactory level of accuracy can be obtained. Second, the results of the parametrical study performed here are in good agreement with the data published in the literature, especially as far as the primary and secondary resonances are concerned. In addition, jump-up and jump-down frequencies were observed and quantified, and the shape of the frequency responses shows the existence of good agreement with the results obtained using a softening or hardening damped Duffing oscillator depending on the strain law of the shell material. In addition, the HBM can be used as a predictive tool to anticipate the hardening or softening behavior of the (encapsulated) microbubble in its host fluid, to distinguish between linear and nonlinear bubble responses depending on the amplitude of the forcing pressure exerted, and to estimate the damping of each harmonic component depending on the viscous properties of the host medium and those of the shell material. As far as the stability of the branches is concerned, a little experience with bubble behavior should suffice to be able to follow the relevant trajectory (dynamic response) of a bubble, depending on the type of ultrasound activation (up/down chirps) used. Information about NL behavior is crucial to many applications, such as the production of anti-cavitation fluids, monitoring the void fraction in environmental science and in nuclear coolants (liquid sodium) and designing medical ultrasound contrast agents. Lastly, analysis of bubbles' frequency responses shows that an ultrasound spectroscopic method could be designed in which the jump-up frequency serves as an unambiguous index to be depending on the bubble diameter. Using down/up chirps, the frequency ranges of which encompass the jump-up frequency associated with a given diameter improves the detection signal to noise ratio of a bubble. Sizing [1,10]-μm bubbles is not possible using the so-called "double frequency" techniques, since the sideband components generated fall outside the bandpass of the medical ultrasound transducers available. The theoretical resolution capacity of the present method when dealing with (detecting and characterizing) a bubble measuring 4 μm is greater than 1 μm.

Acknowledgements

References

[1] T.G. Leighton, *The Acoustic Bubble*, Academic Press, London, 1994.
[2] C.E. Brennen, *Cavitation and Bubble Dynamics*, Oxford University Press, 1995.
[3] V.L. Newhouse, P.M. Shankar, Bubble size measurements using the nonlinear mixing of two frequencies, *Journal of the Acoustical Society of America* 75 (1984) 1473–1477.
[4] D. Cathignol, J.Y. Chapelon, V.L. Newhouse, P.M. Shankar, Bubble sizing with high spatial resolution, *IEEE Transactions on Ultrasonics, Ferroelectrics and Frequency Control* 37 (1) (1990) 30–37.
[5] C.X. Deng, F.L. Lizzi, A. Kalisz, A. Rosado, R.H. Silverman, D.J. Soleman, Study of ultrasonic agents using a dual-frequency band technique, *Ultrasound in Medicine and Biology* 26 (5) (2000) 819–831.
[6] C.Y. Wu, J. Tsao, The ultrasonic weak short-pulse response of microbubbles based on a two-frequency approximation, *Journal of the Acoustical Society of America* 114 (5) (2003) 2662–2671.
[7] D.K. Woolf, Bubbles and the air–sea transfer velocity of gases, *Atmosphere* 31 (4) (1993) 517–540.
[8] S. Vagle, D.M. Farmer, A comparison of four methods for bubble size and void fraction measurements, *IEEE Journal of Oceanic Engineering* 23 (3) (1998) 211–222.
[9] T.G. Leighton, D.G. Ramble, A.D. Phelps, The detection of tethered and rising bubbles using multiple acoustic techniques, *Journal of the Acoustical Society of America* 101 (5) (1997) 2626–2635.
[10] T.G. Leighton, D.G. Ramble, A.D. Phelps, C.L. Morphey, P.P. Harris, Acoustic detection of gas bubble in a pipe, *Acustica with Acta Acustica* 84 (5) (1998) 801–814.
[11] Yu.N. Savchenko, Yu.D. Vlasenko, V.N. Semenenko, Experimental investigations of high speed supercavitated flows, *International Journal of Fluid Mechanics Research* 26 (3) (1999) 365–374.
[12] Y.L. Young, S.A. Kinnas, Analysis of supercavitating and surface-piercing propeller flows via BEM, *Computational Mechanics* 32 (2003) 269–280.
[13] K.S. Suslick, S.E. Skrabalak, Sonocatalysis, in: G. Ertl, H. Knzinger, F. Schuth, J. Weitkamp (Eds.), *Handbook of Heterogeneous Catalysis*, vol. 4, Wiley-VCH, Weinheim, Germany, 2008, pp. 2006–2017.
[14] R.D. Watkins, L.M. Barrett, J.A. McKnight, Ultrasonic waveguide for use in the sodium coolant of fast reactors, *Nuclear Energy* 27 (1988) 85–89.
[15] B.H. Kim, V.S. Yughay, S.T. Huang, B.H. Kim, J.H. Park, C.S. Choi, Hydrogen bubble characteristics during a water–sodium leak accident in a stream generator, *Journal of Industrial and Engineering Chemistry* 6 (6) (2000) 395–402.
[16] J.C. Buckey, D.A. Knaus, D.L. Alvarenga, M.A. Kenton, P.J. Magari, Dual-frequency ultrasound for detecting and sizing bubbles, *Acta Astronica* 56 (2005) 1041–1047.
[17] N. de Jong, L. Hoff, T. Skotland, N. Bom, Absorption and scatterer of encapsulated gas filled microspheres: theoretical considerations and some measurements, *Ultrasonics* 30 (1992) 95–103.
[18] N. de Jong, L. Hoff, Ultrasound scattering properties of Albunex microspheres, *Ultrasonics* 31 (1993) 175–181.
[19] C.C. Church, The effects of an elastic solid surface layer on the radial pulsations of gas bubbles, *Journal of the Acoustical Society of America* 97 (1995) 1510–1521.
[20] B.A. Angelsen, L. Hoff, T.F. Johansen, Simulation of gas bubble scattering for large Mach-number IEEE, in: *Ultrasonics Symposium Proceedings*, 2000, pp. 505–508.
[21] L. Hoff, P.C. Sontum, J.M. Hovem, Oscillations of polymeric microbubbles: effect of the encapsulating shell, *Journal of the Acoustical Society of America* 107 (4) (2000) 2272–2280.

[22] X. Yang, C.C. Church, A model for the dynamics of gas bubbles in soft tissue, *Journal of the Acoustical Society of America* 118 (2005) 3595–3606.
[23] P. Marmottant, S. Van der Meer, M. Emmer, M. Versluis, N. de Jong, S. Hilgenfeldt, D. Lohse, A model for large amplitude oscillations of coated bubbles accounting for buckling and rupture, *Journal of the Acoustical Society of America* 118 (6) (2005) 3499–3505.
[24] K. Tsiglifis, N.A. Pelekasis, Nonlinear radial oscillations of encapsulated microbubbles subject to ultrasound: the effect of membrane constitutive law, *Journal of the Acoustical Society of America* 123 (2008) 4059–4070.
[25] S.M. Van der Meer, B. Dollet, M.M. Voormolen, C.T. Chin, A. Bouakaz, N. de Jong, M. Versluis, D. Lohse, Microbubble spectroscopy of ultrasound contrast agents, *Journal of the Acoustical Society of America* 121 (2007) 648–656.
[26] A.A. Doinikov, J.F. Haac, P.A. Dayton, Resonance frequencies of lipid-shelled microbubbles in the regime of nonlinear oscillations, *Ultrasonics* 49 (2) (2009) 263–268.
[27] P.D. Krishna, P.M. Shankar, V.L. Newhouse, Subharmonic generation from ultrasonic contrast agents, *Physics in Medicine and Biology* 44 (1999) 681–694.
[28] P.M. Shankar, P.D. Krishna, V.L. Newhouse, Subharmonic backscattering from ultrasound contrast agent, *Journal of the Acoustical Society of America* 106 (4) (1999) 2104–2110.
[29] F.A. Duck, Nonlinear acoustics in diagnostic ultrasound, *Ultrasound in Medicine and Biology* 28 (2002) 1–18.
[30] H. Zheng, O. Mukdadi, R. Shandas, Theoretical predictions of harmonic generation from submicron ultrasound contrast agents for nonlinear biomedical ultrasound imaging, *Physics in Medicine and Biology* 51 (2006) 557–573.
[31] Y. Lee, M.F. Hamilton, Time-domain modelling of pulsed finite-amplitude sound beams, *Journal of the Acoustical Society of America* 97 (1995) 906–917.
[32] J.G. Borsboom, A. Bouakaz, M. Versluis, N. de Jong, Harmonic chirp imaging method for ultrasound contrast agent, *IEEE Transactions on Ultrasonics, Ferroelectrics and Frequency Control* 52 (2) (2005) 241–249.
[33] N. de Jong, A. Bouakaz, F.J. Ten Cate, Contrast harmonic imaging, *Ultrasonics* 40 (2002) 567–573.
[34] A. Bouakaz, S. Frigstad, F.J. Ten Cate, N. de Jong, Improved contrast to tissue ratio at higher harmonics, *Ultrasonics* 40 (2002) 575–578.
[35] A.D. Phelps, T.G. Leighton, High resolution bubble sizing through detection of the subharmonic response with a two frequency technique, *Journal of the Acoustical Society of America* 99 (4) (1996) 1985–1992.
[36] F. Frosberg, W.T. Shi, B.B. Goldberg, Subharmonic imaging of contrast agents, *Ultrasonics* 38 (2000) 93–98.
[37] C. Leavens, R. Williams, F.S. Foster, M.D. Sherar, Golay pulse encoding for microbubble contrast imaging with ultrasound, *IEEE Transactions on Ultrasonics, Ferroelectrics and Frequency Control* 54 (10) (2007) 2082–2090.
[38] ⟨http://manlab.lma.cnrs-mrs.fr/⟩ Manlab is a Matlab package for interactive continuation and bifurcation analysis of non linear systems of equations (date last viewed 4/15/09).
[39] B. Cochelin, C. Vergez, A high order purely frequential harmonic balance formulation for continuation of periodic solutions, *Journal of Sound and Vibration* 324 (2009) 243–262.
[40] W. Lauterborn, Numerical investigation of nonlinear oscillations of gas bubbles in liquids, *Journal of the Acoustical Society of America* 59 (1976) 283–293.
[41] H.G. Flynn, in: W.P. Mason (Ed.), *Physical Acoustics*, vol. 1B, Academic Press, 1964, pp. 57–172 (Chapter 9).
[42] J.B. Keller, M. Miksis, Bubble oscillations of large amplitude, *Journal of the Acoustical Society of America* 68 (1980) 628–633.
[43] A.H. Nayfeh, *Perturbation Methods*, John Wiley & Sons Inc., NY, 1973.
[44] A.H. Nayfeh, D.T. Mook, *Nonlinear Oscillations*, John Wiley & Sons Inc., NY, 1995, Wiley-VCH, Weinheim, Germany, 2004.
[45] A.H. Nayfeh, W.S. Saric, Non-linear acoustic response of a spherical bubble, *Journal of Sound and Vibration* 30 (4) (1973) 445–453.
[46] A. Francescutto, R. Nabergoj, Steady-state oscillations of gas bubbles in liquids: explicit formulas for frequency response curves, *Journal of the Acoustical Society of America* 73 (1983) 457–460.
[47] J.S. Allen, R.A. Roy, Dynamics of gas bubbles in viscoelastic fluids. I. Linear viscoelasticity, *Journal of the Acoustical Society of America* 107 (2000) 3167–3178.
[48] A. Prosperetti, Nonlinear oscillations of gas bubbles in liquids: steady-state solutions, *Journal of the Acoustical Society of America* 56 (1974) 878–885.
[49] D.B. Khismatullin, A. Nadim, Radial oscillations of encapsulated microbubbles in viscoelastic liquids, *Physics of Fluids* 14 (10) (2002) 3534–3557.
[50] A. Shima, T. Tsujino, H. Nanjo, Nonlinear oscillations of gas bubbles in viscoelastic fluids, *Ultrasonics* 24 (3) (1986) 142–147.
[51] O.M. Mukdadi, H.-B. Kim, J. Hertzberg, R. Shandas, Numerical modeling of microbubble backscatter to optimize ultrasound particle image velocimetry imaging: initial studies, *Ultrasonics* 42 (10) (2004) 1111–1121.
[52] B. Cochelin, A path-following technique via an asymptotic numerical method, *Computers and Structures* 53 (5) (1994) 1182–1192.
[53] E.A. Neppiras, Acoustic cavitation, *Physics Reports* 61 (3) (1980) 159–251.
[54] M.J. Brennan, I. Kovacic, A. Carrella, T.P. Waters, On the jump-up and jump-down frequencies of the Duffing oscillator, *Journal of Sound and Vibration* 318 (2008) 1250–1261.
[55] L. Liu, J.P. Thomas, E.H. Dowell, P. Attar, K.C. Hall, A comparison of classical and high dimensional harmonic balance approaches for a Duffing oscillator, *Journal of Computational Physics* 215 (2006) 298–320.
[56] R.B. Robinson, R.H. Buchanan, Undamped free pulsations of an ideal bubble, *Proceedings of the Physical Society, Section B* 69 (9) (1956) 893–900.
[57] G. Houghton, Theory of bubble pulsation and cavitation, *Journal of the Acoustical Society of America* 35 (9) (1963) 1387–1393.
[58] A. Bouakaz, N. de Jong, C. Cachard, Standard properties of ultrasound contrast agents, *Ultrasound in Medicine and Biology* 24 (3) (1998) 469–472.
[59] A.D. Phelps, D.G. Ramble, T.G. Leighton, The use of a combination frequency technique to measure the surf zone bubble population, *Journal of the Acoustical Society of America* 101 (4) (1997) 1981–1989.
[60] F.E. Fox, K.F. Hertzfeld, Gas bubbles with organic skin as cavitation nuclei, *Journal of the Acoustical Society of America* 26 (1954) 984–989.
[61] D. Koller, Y. Li, P.M. Shankar, V.L. Newhouse, High speed bubble sizing using the double frequency technique for oceanographic applications, *IEEE Journal of Oceanic Engineering* 17 (1992) 288–291.
[62] A.D. Phelps, T.G. Leighton, Oceanic bubble population measurements using a buoy-deployed combination frequency technique, *IEEE Journal of Oceanic Engineering* 23 (4) (1998) 400–410.
[63] A.M. Sutin, S.W. Yoon, E.J. Kim, I.N. Didenkulov, Nonlinear acoustic method for bubble density measurements in water, *Journal of the Acoustical Society of America* 103 (5) (1998) 2377–2384.
[64] L.A. Ostrovsky, S.N. Gurbatov, I.N. Didenkulov, Nonlinear acoustics in Nizhni Novgorod (a review), *Acoustical Physics* 51 (2) (2005) 114–127.
[65] S. Chen, R. Kinnick, J.F. Greenleaf, M. Fatemi, Difference frequency and its harmonic emitted by microbubbles under dual frequency excitation, *Ultrasonics* 44 (Suppl. 1) (2006) e123–e126.
[66] S.E. Masoy, O. Standal, P. Nasholm, J. Johansen, B. Angelsen, SURF imaging: in vivo demonstration of an ultrasound contrast agent detection technique, *IEEE Transactions on Ultrasonics, Ferroelectrics and Frequency Control* 55 (5) (2008) 1112–1121.